Biomedical Optics EXPRESS

High frame-rate intravascular optical frequency-domain imaging *in vivo*

Han Saem Cho,[1] Sun-Joo Jang,[1,2] Kyunghun Kim,[1,3] Alexey V. Dan-Chin-Yu,[4] Milen Shishkov,[5] Brett E. Bouma,[5] and Wang-Yuhl Oh[1,*]

[1]*Department of Mechanical Engineering, KAIST, 291 Daehak-ro, Yuseong-gu, Daejeon 305-701, South Korea*
[2]*Graduate School of Medical Science and Engineering, KAIST, 291 Daehak-ro, Yuseong-gu, Daejeon 305-701, South Korea*
[3]*Department of Computer Science, KAIST, 291 Daehak-ro, Yuseong-gu, Daejeon 305-701, South Korea*
[4]*Hyunjoo In-Tech, Suite 1901, Daeryung Post Tower 1, 212-8 Guro-dong, Guro-gu, Seoul 152-790, South Korea*
[5]*Wellman Center for Photomedicine, Harvard Medical School and Massachusetts General Hospital, 40 Blossom Street, Boston, Massachusetts 02114, USA*
[*]*woh1@kaist.ac.kr*

Abstract: Intravascular optical frequency-domain imaging (OFDI), a second-generation optical coherence tomography (OCT) technology, enables imaging of the three-dimensional (3D) microstructure of the vessel wall following a short and nonocclusive clear liquid flush. Although 3D vascular visualization provides a greater appreciation of the vessel wall and intraluminal structures, a longitudinal imaging pitch that is several times bigger than the optical imaging resolution of the system has limited true high-resolution 3D imaging, mainly due to the slow scanning speed of previous imaging catheters. Here, we demonstrate high frame-rate intravascular OFDI *in vivo*, acquiring images at a rate of 350 frames per second. A custom-built, high-speed, and high-precision fiber-optic rotary junction provided uniform and high-speed beam scanning through a custom-made imaging catheter with an outer diameter of 0.87 mm. A 47-mm-long rabbit aorta was imaged in 3.7 seconds after a short contrast agent flush. The longitudinal imaging pitch was 34 μm, comparable to the transverse imaging resolution of the system. Three-dimensional volume-rendering showed greatly enhanced visualization of tissue microstructure and stent struts relative to what is provided by conventional intravascular imaging speeds.

OCIS codes: (170.4500) Optical coherence tomography; (170.2150) Endoscopic imaging; (170.3880) Medical and biological imaging.

References and links

1. I. K. Jang, B. E. Bouma, D. H. Kang, S. J. Park, S. W. Park, K. B. Seung, K. B. Choi, M. Shishkov, K. Schlendorf, E. Pomerantsev, S. L. Houser, H. T. Aretz, and G. J. Tearney, "Visualization of coronary atherosclerotic plaques in patients using optical coherence tomography: Comparison with intravascular ultrasound," J. Am. Coll. Cardiol. **39**(4), 604–609 (2002).
2. H. Yabushita, B. E. Bouma, S. L. Houser, H. T. Aretz, I. K. Jang, K. H. Schlendorf, C. R. Kauffman, M. Shishkov, D. H. Kang, E. F. Halpern, and G. J. Tearney, "Characterization of human atherosclerosis by optical coherence tomography," Circulation **106**(13), 1640–1645 (2002).
3. R. A. Leitgeb, C. K. Hitzenberger, and A. F. Fercher, "Performance of fourier domain vs. time domain optical coherence tomography," Opt. Express **11**(8), 889–894 (2003).
4. M. A. Choma, M. V. Sarunic, C. Yang, and J. A. Izatt, "Sensitivity advantage of swept source and Fourier domain optical coherence tomography," Opt. Express **11**(18), 2183–2189 (2003).
5. J. F. de Boer, B. Cense, B. H. Park, M. C. Pierce, G. J. Tearney, and B. E. Bouma, "Improved signal-to-noise ratio in spectral-domain compared with time-domain optical coherence tomography," Opt. Lett. **28**(21), 2067–2069 (2003).
6. S. H. Yun, G. J. Tearney, J. F. de Boer, N. Iftimia, and B. E. Bouma, "High-speed optical frequency-domain imaging," Opt. Express **11**(22), 2953–2963 (2003).
7. S. H. Yun, G. J. Tearney, B. J. Vakoc, M. Shishkov, W. Y. Oh, A. E. Desjardins, M. J. Suter, R. C. Chan, J. A. Evans, I. K. Jang, N. S. Nishioka, J. F. de Boer, and B. E. Bouma, "Comprehensive volumetric optical microscopy *in vivo*," Nat. Med. **12**(12), 1429–1433 (2007).

#197478 - $15.00 USD Received 10 Sep 2013; revised 31 Oct 2013; accepted 10 Dec 2013; published 16 Dec 2013

8. G. J. Tearney, S. Waxman, M. Shishkov, B. J. Vakoc, M. J. Suter, M. I. Freilich, A. E. Desjardins, W. Y. Oh, L. A. Bartlett, M. Rosenberg, and B. E. Bouma, "Three-dimensional coronary artery microscopy by intracoronary optical frequency domain imaging," JACC Cardiovasc. Imaging **1**(6), 752–761 (2008).
9. V. Farooq, B. D. Gogas, T. Okamura, J. H. Heo, M. Magro, J. Gomez-Lara, Y. Onuma, M. D. Radu, S. Brugaletta, G. van Bochove, R. J. van Geuns, H. M. Garcìa-Garcìa, and P. W. Serruys, "Three-dimensional optical frequency domain imaging in conventional percutaneous coronary intervention: the potential for clinical application," Eur. Heart J. **34**(12), 875–885 (2013).
10. T. Okamura, Y. Onuma, H. M. Garcia-Garcia, R. J. van Geuns, J. J. Wykrzykowska, C. Schultz, W. J. van der Giessen, J. Ligthart, E. Regar, and P. W. Serruys, "First-in-man evaluation of intravascular optical frequency domain imaging (OFDI) of Terumo: a comparison with intravascular ultrasound and quantitative coronary angiography," EuroIntervention **6**(9), 1037–1045 (2011).
11. These specifications were identified by the reviewer. The authors could not identify a publicly accessible confirmation.
12. T. Wang, W. Wieser, G. Springeling, R. Beurskens, C. T. Lancee, T. Pfeiffer, A. F. W. van der Steen, R. Huber, and G. van Soest, "Intravascular optical coherence tomography imaging at 3200 frames per second," Opt. Lett. **38**(10), 1715–1717 (2013).
13. C. E. Saxer, J. F. de Boer, B. H. Park, Y. Zhao, Z. Chen, and J. S. Nelson, "High-speed fiber based polarization-sensitive optical coherence tomography of *in vivo* human skin," Opt. Lett. **25**(18), 1355–1357 (2000).
14. S. H. Yun, G. J. Tearney, J. F. de Boer, and B. E. Bouma, "Removing the depth-degeneracy in optical frequency domain imaging with frequency shifting," Opt. Express **12**(20), 4822–4828 (2004).
15. B. H. Park, M. C. Pierce, B. Cense, and J. F. de Boer, "Real-time multi-functional optical coherence tomography," Opt. Express **11**(7), 782–793 (2003).
16. W. Y. Oh, S. H. Yun, B. J. Vakoc, G. J. Tearney, and B. E. Bouma, "Ultrahigh-speed optical frequency domain imaging and application to laser ablation monitoring," Appl. Phys. Lett. **88**(10), 103902 (2006).
17. W. Y. Oh, B. J. Vakoc, M. Shishkov, G. J. Tearney, and B. E. Bouma, ">400 kHz repetition rate wavelength-swept laser and application to high-speed optical frequency domain imaging," Opt. Lett. **35**(17), 2919–2921 (2010).
18. W. Wieser, B. R. Biedermann, T. Klein, C. M. Eigenwillig, and R. Huber, "Multi-megahertz OCT: High quality 3D imaging at 20 million A-scans and 4.5 GVoxels per second," Opt. Express **18**(14), 14685–14704 (2010).
19. M. Shishkov, B. Bouma, I. Jang, D. Kang, H. Aretz, S. Houser, T. Brady, K. Schlendorf, and G. Tearney, "Optical coherence tomography of coronary arteries in vitro using a new catheter," in *Biomedical Optical Spectroscopy and Diagnostics* (Optical Society of America, 2000).
20. M. S. Shishkov, G. J. Tearney, and B. E. Bouma, "Scultpured optical fiber tips for narrow diameter optical catheters," in *Biomedical Topical Meeting* (Optical Society of America, 2004).
21. J. Li, M. de Groot, F. Helderman, J. Mo, J. M. Daniels, K. Grünberg, T. G. Sutedja, and J. F. de Boer, "High speed miniature motorized endoscopic probe for optical frequency domain imaging," Opt. Express **20**(22), 24132–24138 (2012).
22. T. Okamura, Y. Onuma, H. M. Garcia-Garcia, N. Bruining, and P. W. Serruys, "High-speed intracoronary optical frequency domain imaging: Implications for three-dimensional reconstruction and quantitative analysis," EuroIntervention **7**(10), 1216–1226 (2012).

1. Introduction

Intravascular optical coherence tomography (OCT) provides high-resolution (5–10 μm axial, 20–40 μm transverse resolution) cross-sectional images of vascular morphology through an endoscopic imaging catheter [1]. Among a number of imaging modalities that have been investigated for studies of cardiovascular diseases, only OCT provides sufficient resolution to visualize the majority of clinically important microstructures of atherosclerotic plaques [2]. However, need for removing intraluminal blood for clear visualization of the vessel wall has limited clinical applicability of OCT. Due to its relatively slow image acquisition speed, the conventional time-domain OCT (TD-OCT) allows visualization of only a short segment of the vessel following proximal balloon occlusion or nonocclusive saline or contrast agent flush. Taking advantage of the high detection sensitivity of optical frequency-domain imaging (OFDI), a second-generation OCT technology [3–6], comprehensive imaging of a long coronary segment *in vivo* was recently demonstrated with a short and nonocclusive flush [7]. Three-dimensional (3D) visualization of coronary microstructures reconstructed from comprehensive intracoronary imaging became possible and has been utilized as a useful complementary tool to the 2D cross-sectional OCT images [8, 9]. While 3D-OCT has shown promise in several applications including the identification of anatomic features, the effects of percutaneous coronary intervention (PCI), and the assessment of stent struts and their apposition condition, true high-resolution 3D visualization has not been achieved for a long coronary segment since longitudinal spatial resolution is several times poorer than the cross-

#197478 - $15.00 USD Received 10 Sep 2013; revised 31 Oct 2013; accepted 10 Dec 2013; published 16 Dec 2013

sectional resolution due to insufficient imaging speed. Imaging speed of intravascular OFDI is determined by two separate factors, i.e., the image acquisition speed of the OFDI system and the scanning speed of the imaging catheter. Although the fastest intravascular OCT systems have successfully introduced 3D visualization of coronary arteries with an imaging catheter using a proximal scanning fiber-optic rotary junction (FRJ), their imaging speed has been limited to 100 frames/s (MGH OFDI system (512 A-lines/frame)) [8, 9], 160 frames/s (Terumo OFDI system (512 A-lines/frame), Terumo Corp.) [9, 10], or 180 frames/s (Ilumien Optis system (500 A-lines/frame), St. Jude Medical, Inc.) [11] mainly due to the scanning speed of the imaging catheter. Higher frame-rate systems would yield higher longitudinal resolution, cardiac motion artifact reduction, and minimization of the amount of flushing liquid to avoid potential flush-induced complications including contrast-induced myocardial ischemia, nephropathy, and ventricular arrhythmia. Recent demonstration of high-speed coronary artery tissue imaging *ex vivo* with an imaging catheter using a high-speed micro-motor (3,200 fps) shows that distal scanning can also be a promising approach for high-speed intracoronary imaging, although further optimization is needed for *in vivo* imaging, including shortening the distal rigid length and reducing the diameter of the catheter [12].

In this paper, we present high speed *in vivo* intravascular OFDI at a frame rate of 350 images per second (692 A-lines/frame). A short cavity length high-speed wavelength-swept laser enables OFDI imaging at an A-line rate of 242.8 kHz, and a custom-built high-speed and high-precision FRJ spins the imaging catheter at a rate of 350 revolutions per second while maintaining high optical transmission from the stationary system to the rotating catheter. A 4.5-cm-long aorta of a New Zealand white rabbit was imaged *in vivo* in 3.7 seconds following a contrast agent flush. The longitudinal pitch was 34 μm, which is comparable to the transverse resolution of the OFDI system. Three-dimensional reconstruction shows much better visualization of the microstructures of the vessel wall and a stent compared to what is provided by a conventional 200 μm longitudinal pitch.

2. High frame-rate intravascular OFDI system

2.1 System configuration

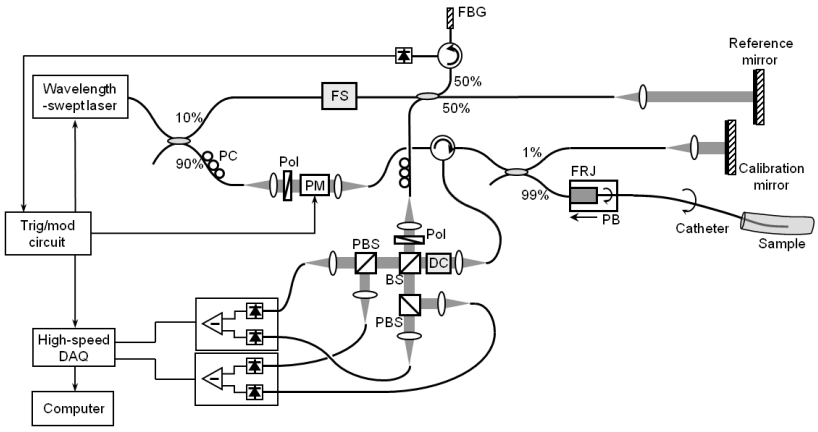

Fig. 1. Schematic diagram of the high frame-rate intravascular OFDI system. PC, polarization controller; FBG, fiber Bragg grating; Pol, polarizer; PM, polarization modulator; FRJ, fiber-optic rotary junction; PB, pull-back; FS, acousto-optic frequency shifter; DC, AMTIR dispersion compensator; BS, beam splitter; PBS, polarization beam splitter.

Figure 1 depicts the high-speed intravascular OFDI system. A wavelength-swept laser constructed using a fiber-based tunable Fabry-Perot filter and a semiconductor optical amplifier (SOA) was used as a light source of the system, providing a wavelength sweep range of 116 nm centered at 1290 nm and a sweep repetition rate of 242.8 kHz. The laser output power was 62 mW and the instantaneous linewidth was measured to be 0.17 nm,

#197478 - $15.00 USD Received 10 Sep 2013; revised 31 Oct 2013; accepted 10 Dec 2013; published 16 Dec 2013

which corresponds to an axial ranging depth of 4.3 mm (the range over which sensitivity remains within 6 dB of that at zero delay). Ninety percent of the laser output is directed to the sample arm and the remaining ten percent is directed to the reference arm of the system interferometer, respectively. Inter A-line polarization modulation is implemented for the polarization sensitive imaging with a polarization modulator (Newport 4104) placed in the sample arm [13]. While most of the sample arm light is directed to the imaging catheter through a fiber-optic rotary junction (FRJ), 1% of it is tapped to generate a signal for laser sweep interpolation and numerical dispersion compensation. An acousto-optic frequency shifter (AOFS, Brimrose Inc. AMF-85-1300) running at 85 MHz was used in the reference arm to remove depth-degeneracy and provide full-range imaging [14]. Half of the reference arm light was then coupled to the reference mirror and another half was directed to a fiber Bragg grating (FBG) for trigger signal generation. A polarization-diverse, balanced detection scheme [15] was implemented for polarization-sensitive imaging, minimizing polarization-dependent signal fading and speckle reduction. Balanced detection provides reduction of source RIN and auto-correlation noise. A dummy AMTIR block was placed at the sample arm light input port of the detection setup for dispersion compensation. A linear polarizer placed at the reference arm light input port of the detection setup with a rotation angle of 45 degrees ensures the same reference arm power for each orthogonal polarization channel and the removal of polarization mode dispersion in the interferometer reference path. Signal from each balanced receiver (Thorlabs PDB460C), corresponding to each orthogonal polarization channel, was acquired by a two-channel, high-speed, and high-resolution digitizer (Signatec PX14400, 14 bits) at a rate of 340 MS/s providing top-to-bottom axial imaging range of 5.2 mm. The axial resolution was measured to be 9.2 μm in air and a sensitivity of 102.5 dB was measured using a mirror with a neutral density filter in a dummy sample arm at an A-line rate of 242.8 kHz.

#197478 - $15.00 USD Received 10 Sep 2013; revised 31 Oct 2013; accepted 10 Dec 2013; published 16 Dec 2013

2.2 Short cavity high-speed wavelength-swept laser

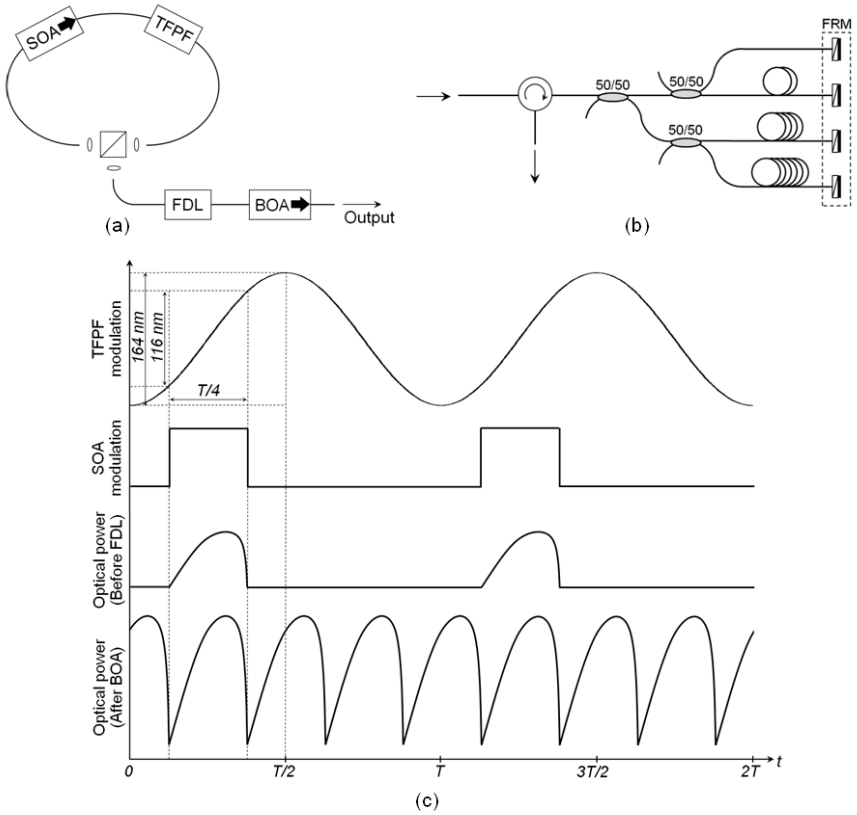

Fig. 2. (a) Schematic diagram of the short cavity length high-speed wavelength-swept laser. SOA, semiconductor optical amplifier; TFPF, tunable Fabry-Perot filter; FDL, fiber delay line; BOA, booster optical amplifier. (b) Fiber delay line using Faraday rotator mirrors (FRMs). (c) Modulation, cut and paste, and booster amplification scheme.

Figure 2(a) shows schematic of the wavelength-swept laser. An SOA (Covega BOA1130) was used as a gain medium of the laser. An isolator integrated inside the SOA butterfly package ensured unidirectional laser oscillation. An intracavity, fiber-based, tunable Fabry-Perot filter (Lambdaquest FFP-TF) was driven at its first resonant frequency of 60.7 kHz. The laser output was obtained through a free-space beam splitter. The lengths of fiber pigtails of the intracavity devices were minimized to reduce the cavity length and the total air-spaced ring resonator length was 48 cm (33 cm in fiber). The short cavity length ensures long photon intracavity lifetime by reducing the filter wavelength shift per round trip to 28% of the 0.16 nm filter bandwidth [16]. While the filter swept its full free-spectral-range (FSR) of 164 nm, the gain of the intracavity SOA was modulated so that the laser was ON during 25% of the full filter tuning period where the wavelength sweep was most linear, as shown in Fig. 2(c). The resulting output comprised a continuous wavelength sweep over 116 nm at a repetition rate of 60.7 kHz with a 25% duty cycle. Three additional laser scans were replicated, sequentially delayed, and then interleaved by a tree-like structure fiber delay line. Faraday rotator mirrors at the end of each delay spool canceled out any polarization rotation that could arise in the long fiber delay as depicted in Fig. 2(b) [17, 18]. Finally, the 242.8 kHz (60.7 kHz × 4) sweep repetition output was amplified to 62 mW average power by a booster optical amplifier (BOA, Covega BOA1130).

#197478 - $15.00 USD Received 10 Sep 2013; revised 31 Oct 2013; accepted 10 Dec 2013; published 16 Dec 2013

2.3 Rotary junction

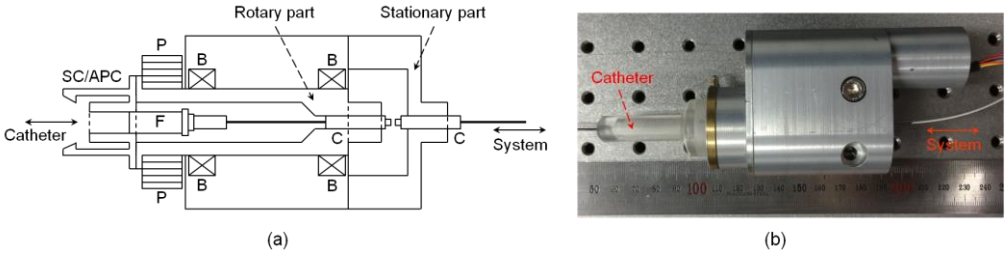

Fig. 3. Fiber-optic rotary junction. (a) Schematic diagram of the core optical junction part of the FRJ. P, pulley; F, angle-polished ceramic ferrule; B, bearing; C, fiber-pigtailed collimator. (b) Fiber-optic rotary junction unit assembled and connected to an imaging catheter.

For rapid beam scanning, we built a high-speed and high-precision fiber-optic rotary junction (FRJ) as shown in Fig. 3. The FRJ was formed with a pair of fiber-pigtailed collimators aligned to each other, where one of them was permitted to spin around its axis [19]. Both stationary and rotary collimator holders were fabricated by high-precision machining. Two high-speed and high-precision bearings were used between the stationary and the rotary parts. The size of the rotary part was minimized in both radial and axial directions to reduce its moment of inertia, while maintaining the strength and the rotational stability. We also used titanium for the rotary part for the same reason. The length of the titanium rotary part was 3.4 cm and the fiber-pigtailed-collimator/ferrule part rotating with the rotary part was 3.8 cm long. The rotary part was driven by a high-speed and high-precision brushless DC-servomotor (Faulhaber 2057S(024B)) through a timing belt and a pulley. The spinning collimator was aligned in a way that the collimating beam remained on the rotational axis. The stationary collimator was then brought close to the rotary collimator and was aligned to obtain higher than 80% coupling over 360 degree rotation of the rotary collimator. The other end of the optical fiber connected to the rotary collimator was angle-polished with a ceramic ferrule and connected to an SC/APC mating sleeve. For pullback, the FRJ unit was mounted on a motorized translation stage (Zaber T-LSQ-075B).

2.4 Imaging catheter

We fabricated a ball lens-based imaging catheter [19, 20]. The imaging optics consisted of a 1.65-m-long single-mode fiber (SMF) with a polyimide jacket (cladding diameter = 125 μm, jacket diameter = 155 μm), a short length coreless fiber attached to the distal tip of the SMF, and a ball lens formed at the tip of the coreless fiber. The length of the coreless fiber and the curvature of the ball lens, which control the characteristics of the imaging beam, were predetermined using a Gaussian beam propagation simulation. Because the beam propagating in transverse plane experiences the curved sheath and water (or contrast agent) as a concave lens, as depicted in Fig. 4(b), tighter focusing by the ball lens in the transverse plane was needed to avoid an astigmatic focus. The ideal lens surface was therefore ellipsoidal. A coreless fiber was fusion-spliced to SMF, and was cleaved to a predetermined length. Then the distal end of the coreless fiber was heated while being translated in a tungsten filament furnace to form a ball lens. We adjusted the translation length and speed, temperature of the filament, and the duration of heating empirically to form the optimal ellipsoidal lens. All of the ball lens fabrication process was performed in a computer-controlled fusion splicing workstation (Vytran FFS-2000). We verified that the lens was fabricated as designed by measuring the transverse and coronal radii of the ball lens and the distance between the SMF/coreless fiber interface and the tip of the ball lens. Performance of the fabricated imaging optics calculated through the Gaussian beam propagation simulation with the measured parameters is summarized in Table 1. To obtain a side-looking catheter, the distal tip of the ball lens was mechanically polished. The angle between the fiber axis and the polished surface was 40 degree as shown in Fig. 4(c), which properly steered the imaging

#197478 - $15.00 USD Received 10 Sep 2013; revised 31 Oct 2013; accepted 10 Dec 2013; published 16 Dec 2013

beam to the vessel wall while also reducing strong back reflection from the surface of the catheter sheath. The fabricated imaging optics were then enclosed within a 3-layer torque coil (Asahi-Intecc) and secured with epoxy. A hypotube with a window was attached to the distal tip of the torque coil by laser welding to protect the imaging optics as shown in Fig. 4(d). The distal rigid length of the catheter is 3 mm, which is the length of the protective hypotube. The proximal tip was terminated with an SC/APC connector. The whole imaging catheter was spun in the stationary sheath with a transparent distal imaging window of 0.87 mm outer diameter.

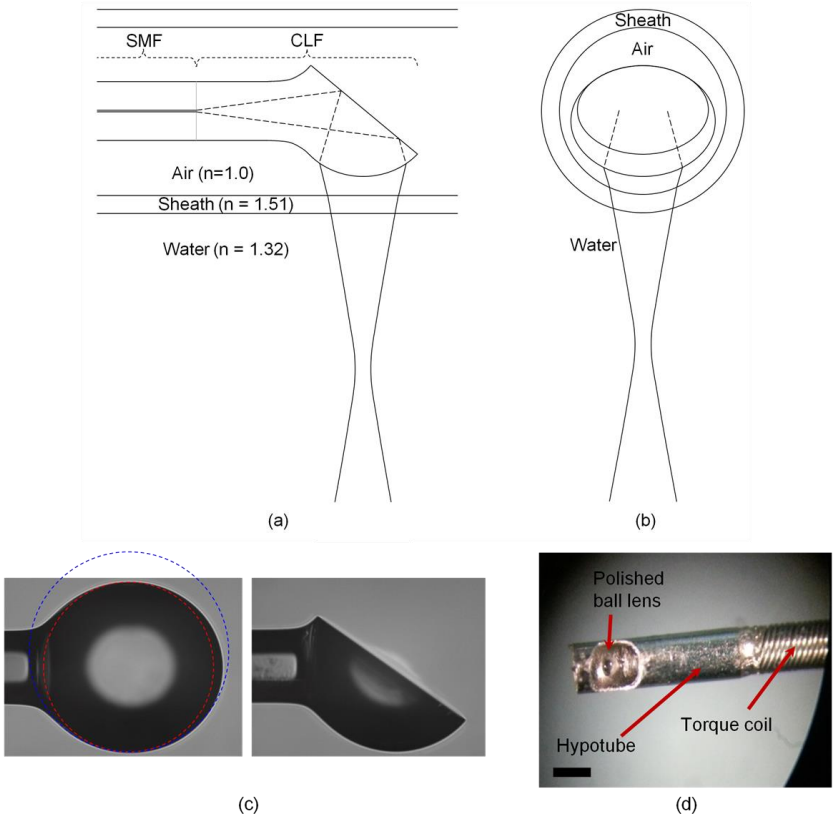

Fig. 4. Schematic of the imaging ball lens, (a) side view (coronal plane beam propagation), and (b) front view (transverse plane beam propagation). SMF, single mode fiber; CLF, coreless fiber. (c) Fiber-optic ball lens fabricated, before and after polishing. The red circle represents transverse plane curvature and the blue circle represents coronal plane curvature of the lens. (d) Ball lens enclosed within a 3-layer torque coil with a hypotube at the distal end, Scale bar: 0.5 mm.

Table 1. Performance of the imaging ball lens

	Transverse plane	Coronal plane
Spot size at beam waist ($1/e^2$)	28.5 μm	29.6 μm
Distance from sheath outer surface to beam waist	1.29 mm	1.69 mm
2 × Rayleigh range	1.31 mm	1.39 mm
Range with spot size $<50\,\mu m$	1.87 mm	1.90 mm

#197478 - $15.00 USD Received 10 Sep 2013; revised 31 Oct 2013; accepted 10 Dec 2013; published 16 Dec 2013

3. Imaging

Fig. 5. OFDI image of human fingers acquired at a rate of 350 frames/s (21,000 rpm) through a spinning imaging catheter (Media 1).

To evaluate the catheter-based OFDI system built, we imaged human fingers with the imaging catheter rotating at a rate of 21,000 revolutions per minute under computer control, yielding a frame rate of 350 images/s (692 A-lines/frame). As shown in Fig. 5, layers of human finger were well visualized without showing any significant non-uniform rotation distortion through the curved imaging catheter with approximately 5-cm minimum bending radius [21].

Intravascular imaging of a rabbit aorta was performed *in vivo*. The animal experiment protocol was approved by the Institutional Animal Care and Use Committee (IACUC) of Korea Advanced Institute of Science and Technology (KAIST). We prepared a 3.5–4 kg New Zealand white rabbit. The rabbit was anesthetized by intramuscular injection of zolazepam/tiletamine 25 mg/kg and xylazine 10 mg/kg. A 4 cm midline incision was made in the anterior neck of a rabbit. After exposure of the right common carotid artery (CCA), a vascular clip (bulldog clip) was placed on the proximal part of the CCA. A permanent ligation was performed with 3-0 silk in the distal part of the CCA. A 22-G Angiocath (BD Medical, Sandy, Utah, USA) was inserted 5 mm proximal to the distal ligation and a 0.035" guide-wire was inserted into the CCA by the modified Seldinger method. The puncture hole was enlarged using microscissors and a 6-Fr guiding catheter was advanced into the descending aorta and connected with a Y-connector. A 0.014" guide-wire was inserted into the guiding catheter and a drug-eluting stent (Promus Element™, Boston, Scientific, MA, USA) was implanted into the abdominal aorta. The OFDI imaging catheter was inserted into the aorta over the guide-wire. Iodinated radiographic contrast (Pamiray 370: Iopamidol 755 mg/ml (370 mg as iodine)) was manually injected at 3 ml/s through the side port of the Y-connector and the rotating imaging catheter was simultaneously pulled back for volume image recording. After imaging, the rabbit was euthanized by exsanguination.

#197478 - $15.00 USD Received 10 Sep 2013; revised 31 Oct 2013; accepted 10 Dec 2013; published 16 Dec 2013

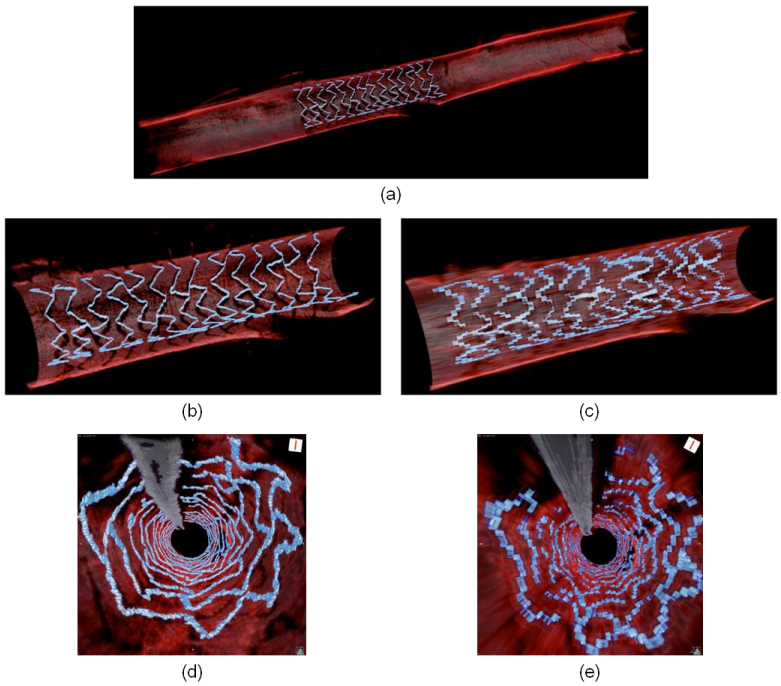

Fig. 6. Three-dimensional, volume-rendered intravascular OFDI images acquired *in vivo*. (a) Longitudinal cutaway view of a 45-mm-long rabbit aorta acquired in 3.7 s with an imaging pitch of 34 μm (350 frames/s). Longitudinal cutaway views of the stented vessel segment with (b) 34 μm and (c) 200 μm longitudinal pitches, respectively. (d) Fly-through views of the same stented vessel segment with (d) 34 μm and (e) 200 μm longitudinal pitches, respectively.

A series of circular sections were acquired at 350 frames/s with a pitch of 34 μm during a pullback of 45 mm in 3.7 s (12 mm/s). A three-dimensional reconstruction was obtained utilizing volume-rendering software (OsiriX 5.6, The OsiriX Foundation) as shown in Fig. 6. For comparison, we also imaged the same portion of the aorta with a slower frame rate but the same pullback speed, generating images with conventional 200 μm longitudinal pitch. In both fly-through and cutaway longitudinal views, improved visualization of the vessel is clearly evident with the faster system. Thanks to an approximately six-fold finer longitudinal resolution (34 μm (Fig. 6(b) and 6(d)) vs. 200 μm (Fig. 6(c) and 6(e))) with the high frame-rate system, the stent strut microstructure was better appreciated with almost no discontinuity. The orifice of the side branch was also clearly visualized. It is worth noting that we can easily identify the malapposed struts from the shadow on the vessel wall in the 3D cutaway longitudinal view [9]. Unlike intracoronary imaging where the artifact due to the cardiac motion especially in systolic period is significant, we did not observe any severe motion artifact in the images mainly because aorta experiences very little cardiac-induced motion [22]. This system can also provide a pullback speed of 72 mm/s when we image with the conventional longitudinal pitch of 200 μm. High-speed pullback with high frame-rate OFDI can reduce cardiac motion-induced artifact by potentially performing whole coronary artery imaging within a single cardiac cycle.

4. Conclusion

A high frame-rate OCT system that can perform intravascular imaging *in vivo* is desirable for many reasons, including higher longitudinal resolution, cardiac motion artifact reduction, and minimization of amount of flushing liquid required for clinical applications. In this paper, we have presented a high frame-rate intravascular OFDI system, and have demonstrated true high-resolution 3D intravascular imaging *in vivo*. The high-speed OFDI system, the high-speed and high-precision FRJ, and the thin and high-performance imaging catheter enabled

#197478 - $15.00 USD Received 10 Sep 2013; revised 31 Oct 2013; accepted 10 Dec 2013; published 16 Dec 2013

intravascular OFDI imaging of a rabbit aorta *in vivo* at an imaging rate of 350 frames/s. The microstructure of the vessel and stent struts was clearly visualized with a longitudinal pitch of 34 μm. We believe that the superior visualization capability of high frame-rate intravascular OFDI systems will play an important role in future clinical studies, providing enhanced plaque characterization, and improved evaluation of PCI, thereby increasing the clinical utility of OCT. For clinical high frame-rate intracoronary imaging, further optimization should follow to ensure NURD-free imaging through tortuous structures like coronary arteries.

Acknowledgments

This research was supported in part by the NRF of Korea, grant 2010-0017465, by the MSIP of Korea, grant GFP/(CISS-2012M3A6A6054200) and grant NIPA-2013-H0401-13-1007, and by the NIH, grant P41 EB015903.